Design methodology for a prototype helical receiver adopted in the MOSAIC solar bowl system

Design Methodology for a Prototype Helical Receiver Adopted in the MOSAIC Solar Bowl System

Mattia Cagnoli[1], Jens Jørgen Falsig[2], Marcelino Sanchez[3], Iñigo Pagola[3], Adrian Peña-Lapuente[3], Laura Savoldi[1], Cristóbal Villasante[4] and Roberto Zanino[1,*]

[1] *Dipartimento Energia, Politecnico di Torino, Corso Duca degli Abruzzi 24, 10129 Torino, Italy*
[2] *Aalborg CSP, Hjulmagervej 55, 9000 Aalborg, Denmark*
[3] *National Renewable Energy Center (CENER), Ciudad de la Innovación, 7, 31621 Sarriguren (Navarra), Spain*
[4] *IK4-TEKNIKER, Calle Iñaki Goenaga 5, 20600 Eibar (Gipuzkoa), Spain*

*corresponding author: roberto.zanino@polito.it

Abstract

This paper presents the design methodology of the receiver developed within the MOSAIC H2020 project, which proposes and is now commissioning an innovative solar bowl system, also known as SRTA (Spherical Reflector Tracking Absorber), aiming at reducing the Levelized Cost Of Electricity (LCOE) with respect to the most popular Concentrated Solar Power (CSP) technologies. The solar bowl technology consists of a fixed (non-tracking) spherical mirror that concentrates the solar radiation on a receiver, which moves tracking the sun. Past investigations of this technology were limited so far, although it can potentially reduce both capital and operational costs because of the adoption of a non-tracking mirror, which imposes special attention and care in the design of the receiver. The design methodology for the MOSAIC receiver presented in the paper consists of three main steps. First, a preliminary study is performed, which results in the choice of the helical receiver configuration among other alternatives. Second, the "macroscopic" features of the chosen configuration, which define the external size of the receiver, are determined, based on an ad-hoc developed optical model, adopting the Monte-Carlo ray-tracing technique implemented in the Tonatiuh software to compute the heat flux distribution over the receiver surface. Third, and last, the "microscopic" design parameters, i.e. the absorber tubes diameter and the number of parallel threads in the helix, are optimized by means of an ad-hoc developed quasi-3D thermal-fluid-dynamic model. This model solves the 1D mass, momentum and energy balance of the coolant and the lumped heat conduction problem in the solid wall, calculating the heat losses and, consequently, the thermal performance of the receiver. Finally, an example of application of the model to the analysis of transient operation is presented: the resulting rate of change of the tube wall temperature in the case of a fast start-up determines the minimum transient duration required to avoid excessive thermal stresses on the receiver.

Keywords: Solar Thermal, Solar Bowl, Helical Receiver, Ray Tracing, Modelica

1 Introduction

The environmental impact of fossil fuel consumption, which consists of the emission of pollutant and greenhouse gasses, imposes to move towards a power production based on renewable sources (IEA International Energy Agency, 2018). Among the different renewable technologies, Concentrated Solar Power (CSP) is very promising because of the abundance of the solar resource and because the thermal power produced can be stored; this allows generating electricity in a dispatchable way exploiting the best selling opportunities of the market.
The working principle of a CSP system consists in concentrating the sunlight by means of one or more mirrors, which typically track the sun, onto a receiver that transfers the energy of the concentrated rays to a heat transfer fluid driving then a conventional Rankine or Brayton cycle.
The most diffuse CSP technology is the parabolic trough system (Islam et al., 2018), which adopts a parabolic collector to concentrate the solar radiation on a linear receiver. However, in the last years the central tower technology is becoming more and more attractive because this point-focus system allows overcoming the limits of the parabolic

trough technology in terms of maximum achievable concentration ratio, although requiring a more accurate solar tracking system (Fernández et al., 2019).

Few CSP systems based on a fixed concentrator and a moving receiver have been proposed so far in the literature. In the 1980s (Texas Tech University, 2019), the solar bowl system was proposed as a CSP technology based on a fixed concentrator, consisting of a stationary spherical concentrator and a tracking receiver. More recently Maatallah et al. (Maatallah et al., 2018) presented a novel CSP system based on a cylindrical mirror placed in a stationary position, while the linear receiver moves tracking the sun. Particularly, Maatallah et al. developed a numerical model to investigate the optical performance of the fixed concentrator and its sensitivity with respect to a set of relevant parameters (rim angle, incidence angle, etc.).

In this paper, an innovative CSP technology, based on the solar bowl concept (also known as SRTA – Spherical Reflector Tracking Absorber), is presented. The solar bowl system consists of a large fixed spherical mirror that focuses the solar radiation in a non-uniform way along a line passing through the sphere center and pointing to the sun (Stine and Geyer, 2001); see Figure 1. The irradiated length along this line is from the surface of the mirror to half of the sphere radius and the peak of the concentrated radiation is reached close to half of the radius (Stine and Geyer, 2001). A cylindrical-shaped receiver, whose axis coincides with the focusing line, collects the reflected solar radiation. The peculiarity of the solar bowl system is that the mirror is fixed, while the receiver moves, tracking the sun; in fact, the focusing line changes its position during the day, because of the apparent movement of the sun in the sky. The fixed mirror represents a key advantage of this technology, since it allows reducing both capital and operational costs, thus leading to a reduction of the levelized cost of electricity (LCOE). On the other hand, the drawback of having a fixed mirror is that part of the reflecting area is in shade depending on the sun position, see Figure 1b, thus limiting the optical performance of the system: the lower the sun is, the higher is the mirror area cut off (i.e., the reflecting surface that is not reached by the sun rays).

The solar bowl technology was not intensely investigated in the past. Fruchter et al. experimentally studied a small-scale solar bowl prototype (aperture diameter equal to 2.52 m) under steady-state conditions, at heat transfer fluid temperatures up to 300 °C; the tracking receiver, supported by a pivot rod, was a cylindrical coil encapsulated in a Pyrex glass cylinder and cooled by mineral oil (Fruchter et al., 1982). A similar work was performed by Cohen (Cohen and Grossman, 2016), using a solar bowl of 2.8 m diameter that adopted as receiver a cylindrical coil encapsulated in a glass tube. The working fluid in this case was water and the main conclusion of this work was that the stationary reflector could be efficiently exploited to produce process heat for domestic or industrial use.

The most significant experiences so far in the field of solar bowl technology are essentially a pilot plant in Crosbyton, Texas (O'Hair and Green, 1992) and the Auroville solar kitchen in India (Van den Akker, 2004).

The Crosbyton solar bowl consisted of a spherical mirror of 19.8 m diameter made of 430 one-square-meter mirrors, (see Figure 2a); it was designed, constructed and operated in the 1980s by the Texas Tech University. A two-axis tracking mechanism, based on a yoke assembly and drive motors, kept the receiver on the focus line. The receiver was cooled with water and it directly produced steam at the outlet section, which was exploited for electricity production. At the end of the seven years of operation, it was concluded that the main losses were due to the cosine effect plus convection and radiation from the receiver towards the environment. Those losses led to a total efficiency that is lower than that of the parabolic trough and solar tower systems; therefore, the cost of the solar bowl system must be lower to make this technology competitive.

The Auroville solar kitchen, see Figure 2b, was commissioned in 1999 and consists of a bowl of 15 meter diameter, made of more than 10'000 small mirrors, that concentrates the solar radiation over a tracking receiver kept on the focal line by means of a computer-controlled pivot mechanism. The heat transfer fluid (HTF) is water and the receiver directly generates steam, which is used for cooking about 1200 meals/day (nominal thermal power 75kW) (Van den Akker, 2004).

The receiver of the Crosbyton pilot plant consisted of two parallel helical absorber tubes wound on an envelope of cylindrical shape (about 13 cm diameter and 5.7 m height (O'Hair and Green, 1992)). Similarly, the receiver of the Auroville solar kitchen is made of a bundle of three parallel helical tubes spiraled around a cylinder; on the very top part of the receiver, the cylinder is replaced with a cone (cone helix) to better capture the concentrated solar radiation.

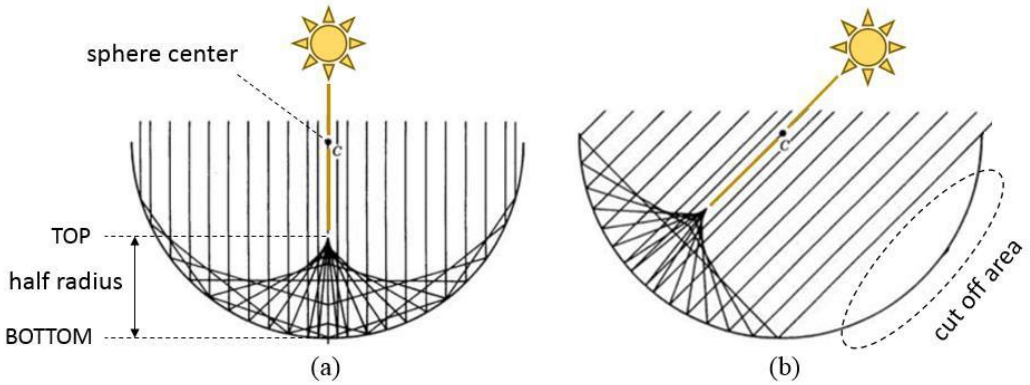

Figure 1. Solar bowl system consisting of a fixed spherical mirror: concentration principle; edited from (Stine and Geyer, 2001). (a) The case in which the sun rays are perfectly perpendicular to the aperture; (b) the case in which the reflecting area is reduced, because the mirror does not track the sun.

(a) (b)

Figure 2. The Crosbyton solar bowl (Texas Tech University, 2019) and (b) the Auroville Solar kitchen (Solar Cookers International, 2019)

A new concept of solar bowl is being investigated in the context of the MOSAIC H2020 project (MOSAIC, 2019). The main innovations are:

- the solar field, which is based on a semi-Fresnel configuration (see Figure 3) ;
- the cable-based tracking system;
- the design, in particular of the receiver, aimed at working with molten salts as HTF and high heat fluxes.

The semi-Fresnel approach has been applied to the solar field to reduce the capital cost and to make the maintenance easier. Instead of implementing a single spherical concentrator, the MOSAIC system implements a set of concentric spheres, leading to a semi-Fresnel configuration. The final configuration of the MOSAIC prototype (see Figure 3), which was established on the base of a cost analysis, consists of portions of 3 concentric spheres that in turn are divided in mirror panels. The outermost ring includes 19 panels, the middle ring has 15 panels, while the innermost portion is made of 6 large panels plus four corner panels of reduced size. The total reflecting area is about 600 m^2. The cost reduction is due to the lower wind load with respect to a conventional solar bowl. In fact, the maximum mirrors height is reduced (most of the solar field is close to the ground level) and the apertures between adjacent mirror panels allow the wind blowing through. The lower wind load implies the possibility to adopt lighter supporting structures reducing in this way the cost. Moreover, the space between the concentric spheres and the mirror panels allows an easy access to the solar field, which makes the maintenance easier.

Regarding the tracking system, unlike previous developments based on heavy and costly tripod configurations, the MOSAIC project aims to develop a much lighter tracking system based on actuated cables suspended by simple low-cost vertical stands. This concept opens a very interesting way to cut the costs, although it can be less stiff. The actual

capacity of this tracking system in reducing the cost while ensuring an accurate tracking will investigated by means of the prototype that is currently under construction.

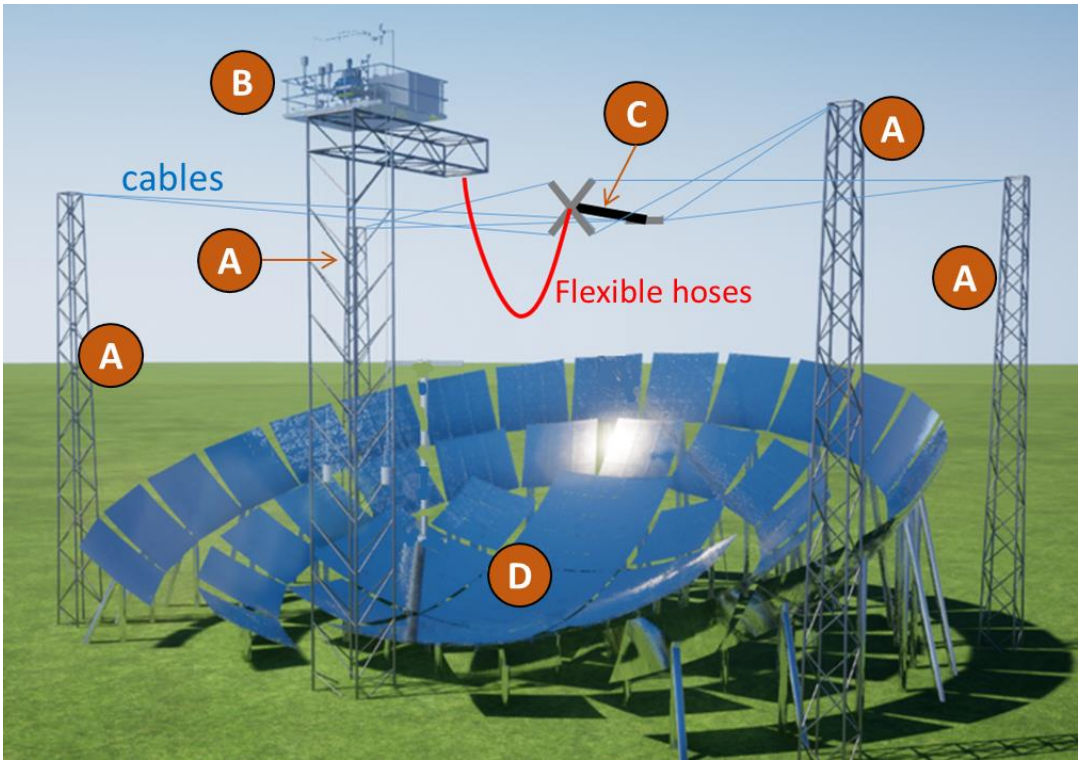

Figure 3. Semi-Fresnel spherical concentrator developed within the MOSAIC project: A) 4 towers for the cable-based tracking system; B) 5th tower for the HTF loop; C) Moving receiver; D): Fixed (Semi-Fresnel) solar field.

Molten salts easily allow integrating a thermal energy storage (TES) in the system since they represents the dominant commercial solution for TES (Fernández et al., 2019), which in turn makes in principle possible to produce dispatchable power according to the demand. Indeed, the presence of a TES to decouple the electricity production from the solar resource is recognized as a key feature to make Concentrating Solar Power (CSP) economically sustainable (IRENA International Renewable Energy Agency, 2018).
To validate the MOSAIC concept, a reduced-scale prototype is being commissioned close to Sangüesa (Spain). The prototype will be operated using silicon oil (maximum temperature 450 °C), to reduce in this first stage the technological risk due to the freezing of the HTF. The methodology and the numerical models (optical and thermal-fluid-dynamic) presented in this paper to design the receiver prototype can be also used to design the full-scale MOSAIC receiver.
The present work focuses on the design of the solar receiver proposed for the MOSAIC prototype, starting from the solar field (section 2), and based on a preliminary study and on the development of an optical plus thermal-fluid-dynamic numerical model and on its application to the analysis of the steady state operation of the system (section 3). In addition, a thermal analysis in transient conditions (fast start-up) will be presented, (section 4) aimed at evaluating the maximum rate of temperature increase of the receiver, which is an important parameter to check its capability to withstand high heat flux changes during fast transients. The novelty of this paper is in the methodology, consisting on an accurate optical (Monte Carlo based) plus thermal (lumped parameter model) numerical analysis, which is applied for the first time, at the best of the authors' knowledge, to the design of a solar bowl receiver.

2 Solar field

The receiver design is strongly conditioned by the particular solar flux distribution that the solar field produces on it. The solar field has been optimized in terms of ratio between construction cost and annual energy obtained, searching

for the best configuration in terms of parameters like tilt of the solar field, number of rings, curvature radius and increase in curvature radius between rings. More detailed information about the solar field optimization are available in (Villasante et al., 2020, 2019).
Taking into account this complexity, in a first approximation the receiver is supposed to be a perfect cylinder and the parametric study is performed using a few analytical formulas implemented in a simple Matlab code.
The solar field is formed by spherical-shaped sections that are discretized and approximated by planes. For each of those sections the reflected rays were calculated using Snell's law

$$n_i * \sin\theta_i = n_r * \sin\theta_r \quad (1)$$

where θ_i and θ_r are the angles of incidence and refraction, while n_i and n_r are the indices of refraction, and considering the varying sun position during the year, which was sampled every minute. For an ideal mirror n_i is equal to n_r since the medium in which the solar rays travel is the same (air), before and after the collision.
The analytical model takes into account the optical losses due to the shadowing produced by the receiver and by the solar field itself and to the blocking caused by the adjacent panels (semi-Fresnel configuration). The sun shape and the quality of the mirrors have not been considered in the analytical model used for this first optimization of the solar field. The rays that are neither blocked nor shadowed will intercept the focal line, where the receiver should be placed. From here, the time-dependent flux incident on the receiver is obtained, and by integrating it along the year, the total flux distribution (in W h/m^2) that can reach the receiver. This information is used to determine the best solar field configuration optimizing the solar field parameters, such radius of the rings, aperture radius, shape radius and concentrator radius. In addition, the annual flux distribution allows determining which areas of the solar field provide a little contribution in terms of annual solar energy collected; these areas can be removed saving capital cost in order to obtain the most cost-efficient configuration.
The final solar field resulting from this optimization exercise is composed by an inner spherical cap and two spherical rings, with curvature radii between 15 m and 17.9 m (see Figure 3). This will define the appearance of the flux footprint on the receiver, due to the properties of the reflection of a spherical mirror.
This kind of mirror ideally produces a sort of caustic curve (McIntosh, 1990), which defines the uppermost point of the receiver that is going to get the radiation reflected from the concentrator. Indeed, that is where the concentration peak occurs. In the case at hand, where the concentrator is defined by the three different curvature radii, the uppermost point for each curvature radius has to be obtained, depending on the receiver radius (see section 3.2 below), which defines the distance to the focal line in which the different caustics are going to be intersected. The optical model well reproduces the peak flux position predicted by the theoretical analysis of the caustic curve.
The semi-Fresnel configuration leads to a strongly uneven flux due to the appearance of three flux peaks at different heights, which, in addition, depend on the sun position. This means that each mirror ring focuses the sun light on a different section of the receiver, depending on the solar incidence angle. In order to illustrate this phenomenon, Figure 4 shows the flux incident on the receiver prototype at the beginning of the day (Figure 4a) and at midday, i.e. 12:00 pm clock time (Figure 4b).

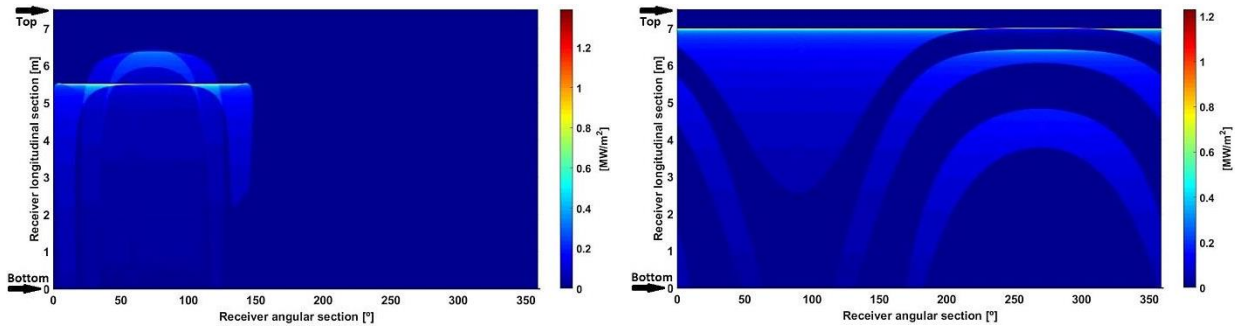

(a) (b)

Figure 4. Flux distribution on the (unwrapped) receiver surface at different times/solar angles on April, 8th. (a) Beginning of the day (08:00 am), (b) midday (12:00 pm clock time).

In Figure 4a, the elevation of the sun is still low and the contributing section of the solar field is small. In addition, that section is the outermost western section, which implies that it is concentrated in only one side of the receiver and,

due to the lower incident position of the outer rings explained with the caustic curve, mainly in a low part of the receiver.
Figure 4b shows the power distribution on the receiver at 12:00 pm. In this case, as the elevation of the sun is higher, the contribution of each ring appears more clearly represented, and it is possible to observe where the peaks of the inner cap and the first ring are.

3 Receiver design – steady-state analysis

This section describes the models developed to design the receiver and presents the results of the simulations performed. First, the general receiver layout is presented; then, the optical and thermal analysis for the optimization of the receiver will be discussed, together with the models developed to carry out the design.

3.1 General layout

As a consequence of the optical properties of a spherical reflector, which concentrates the solar radiation along a line, the receiver will have a cylindrical shape and the axis of the cylinder should be coincident with the focus line. As seen in the previous section, the receiver layout adopted in the previous solar bowl experiences consists of a bundle of parallel helical tubes wound on an envelope of almost cylindrical shape. The use of helical coil as receiver has been already successfully adopted in the CSP field, especially in cavity receivers; see for example (Awasthi and Khan, 2019; Pye et al., 2017). In the MOSAIC project this configuration has been preliminarily compared with two other alternatives; namely, the annular and the external (straight) tubes configurations (see Figure 3). The annular layout was discarded because of the poor thermal performance caused by the very low Reynolds number reachable in the annular region by the HTF (for any reasonable mass flow rate), which results in a laminar flow that strongly penalizes the convective heat transfer to the HTF. The external tubes configuration, instead, could in principle perform as well as the helical one; however, it presents the following drawbacks:

- It makes the gravity-driven drainage of the molten salts inside the receiver difficult to be performed, due to the multi-pass of the HTF in the receiver tubes (up and down). The latter obviously is an issue only in the case of the full scale MOSAIC module, which uses molten salts as HTF, while in the prototype thermal oil is used; however, the prototype is designed considering all the constraints applicable to the full-scale receiver. The multi-pass makes it possible to reach the desired outlet temperature by increasing the residence time in the receiver; in fact, a single pass is not sufficient to reach the outlet temperature without dramatically reducing the mass flow rate (laminar flow). To allow the multi-pass configuration, the tubes are connected at the receiver ends by means of U-junctions (see Figure 5), which are also tricky to be drained by gravity.
- Because of the strongly non uniform heat flux distribution (see Figure 4), the straight pipes in the external tubes configuration will be irradiated in a very uneven way, potentially leading to dangerous hot spots, while the helical configuration ensures that the HTF homogenizes the temperature across the receiver.

The direction of the HTF in the directly irradiated part of the receiver configuration considered here is from the bottom to the top, because of the solar heat flux distribution: as the heat flux increases from the bottom to the top (see section 3.2 below), the HTF entering from the bottom is progressively heated up while flowing along the receiver. On the contrary, if the HTF enters from the top, where the heat flux peak is located, its temperature suddenly increases up to about the target value. Consequently, it flows at high temperature for most of the helical tubes length leading to a higher temperature of the tubes wall (prone to heat losses) with respect to the case in which it is progressively heated. In the helical configuration, the coolant flows from the top of the receiver to the bottom in a straight tube located inside the helix (as shown in Figure 5c), then it flows back in the irradiated helical tubes towards the top part of the receiver. The gap between the helical tubes and the straight tube inside the helix is simply filled with air at atmospheric pressure. The helical configuration can also benefit from the addition of a conical insert on the top part (Figure 5c), as in the Auroville receiver, which allows better intercepting the solar rays reducing the total length of the receiver.
The detailed design of the MOSAIC helical receiver requires 1) an optical model to evaluate the heat flux distribution on the receiver surface depending on the sun position, and 2) a thermal-fluid-dynamic model, which allows estimating the heat losses (i.e., the thermal performance). Both are presented below.
The parameters to be determined in the design process (see also Figure 6) are:

- the "macroscopic" parameters, namely the receiver diameter D and length L, as well as the cone angle θ;
- the "microscopic" parameters, namely the diameter d of the absorber tubes and the number N of parallel threads.

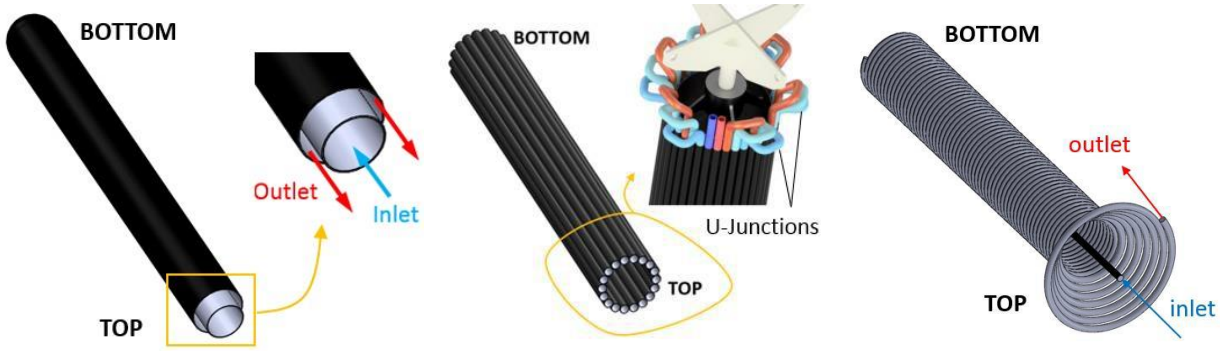

(a) (b) (c)

Figure 5. Alternative concepts initially considered within the MOSAIC project: (a) annular configuration, (b) external tubes with the detail of the U-junctions and (c) helical configuration.

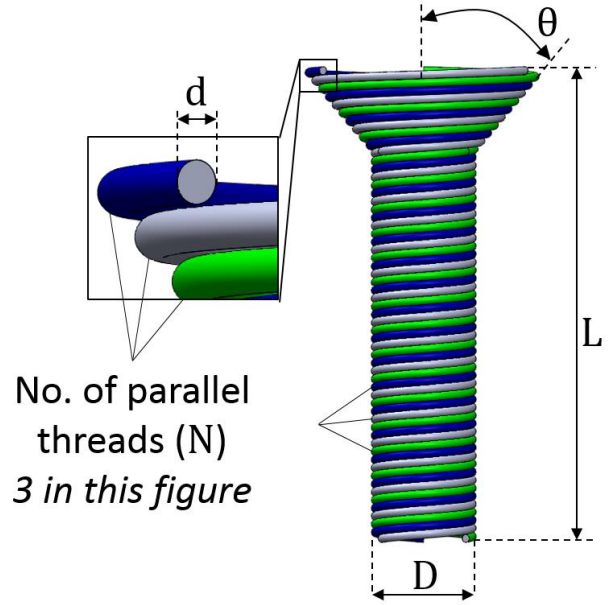

Figure 6. Design parameters: receiver length (L), diameter of the cylindrical part (D), cone angle (θ), diameter of the absorber tubes (d) and number of parallel threads (N)

It is intuitively clear that the macroscopic parameters will be mainly determined by the optical analysis: indeed, the receiver diameter depends mainly on the spillage of the concentrated solar radiation, and the capability to maximize the absorbed power while minimizing the length of the receiver will determine the most promising combinations of receiver length and cone angle. On the other hand, the microscopic parameters will be mainly determined by the thermal analysis, as both the absorber tube diameter and the number of threads affect the Reynolds number of the HTF inside the tubes and therefore the heat transfer coefficient. The absorber tube wall thickness was not included in the design parameters investigated here, rather it was fixed to 1.5 mm on the base of the experience of the MOSAIC receiver manufacturer, considering also the market availability. The absorber tubes are made of Incoloy 800.

On top of these principle modeling considerations, some important practical constraints to be considered in the design process are listed below:

- the receiver diameter cannot be smaller than 0.3 m ($D \geq 0.3$ m), because of the bending process of thin walled tubes;
- the absorber tube diameter cannot be smaller than one inch ($d \geq 1$”), due to the availability on the market;
- the absorber tube slope cannot be smaller than 2°, to ensure the drainage of the receiver by gravity; this in turn gives an upper bound for the cone angle θ;

- the number of parallel threads cannot be smaller than 3 ($N \geq 3$), in order to ensure sufficient space to weld the helical tubes using a cost-effective manufacturing procedure (a single absorber tube length being made of different sections welded together). In addition, N also affects the tubes slope.

Figure 7 summarizes the design methodology presented in this paper and applied to the design of the receiver prototype; however, the same procedure can be applied to the full-scale receiver.

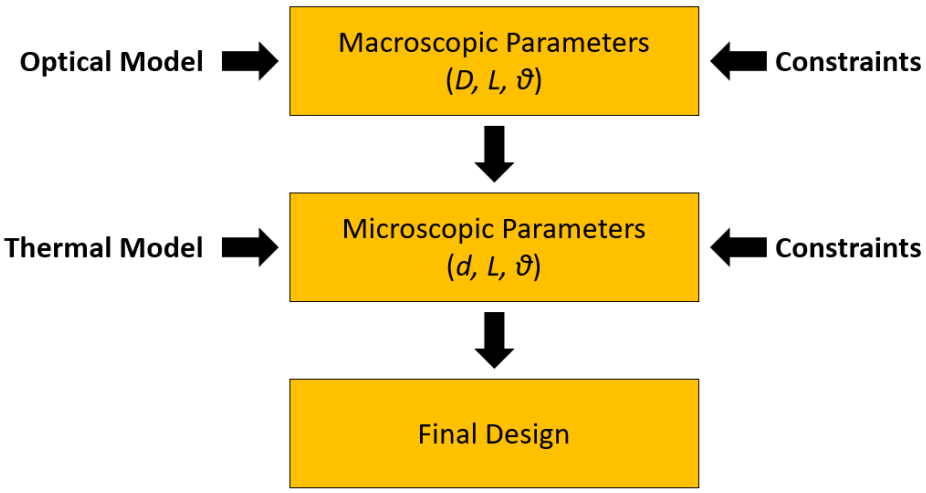

Figure 7. Scheme of the methodology adopted for the receiver design

3.2 Optical analysis

The main objective of the optical analysis of the receiver is to optimize the receiver configuration in order to reduce its size as much as possible, while still capturing most of the energy reflected by the concentrator. For this purpose, Tonatiuh, which is a Monte-Carlo ray-tracing software (Blanco et al., 2005), is utilized to model the optical performance of different receiver configurations. The Buie sunshape model, with circumsolar ratio CSR = 0.02 is applied due to the expected atmospheric cleanliness in the place in which the prototype is being erected. In addition, mirror slope error is taken into account as a normal distribution with sigma slope = 2.5 mrad. The receiver model is based on the approximation of the loops of the helical geometry by a series of tori that share their symmetry axis. Each torus is assumed to be generated by the revolution of a circle of diameter equal to d. The reflectivity of the coating, in this case Pyromark, is included in the model accounting for the angle-dependent refractive properties and performance of the material (Ho et al., 2013). By this, it can be taken into account that the radiation reflected by the Pyromark is not completely wasted, because, due to both the tubular layout and the final upper cone, it can be incident on contiguous loops of the tube and even on other sections of the receiver such as the conic-shaped upper part. It was checked that the computed results are independent by the number of photons simulated.
The computed heat flux distribution along the focus line is strongly non-uniform (see Figure 8), varying from the high heat flux region close to the radius mid-point, decreasing almost exponentially when approaching the mirrors, and vanishing in the section between the center of the spheres and the mid-point to the mirrors. Three peaks can be detected in Figure 8 close to the radius mid-point; these peaks are a consequence of the semi-Fresnel configuration of the concentrator, which consists of 3 mirrors (see Figure 3). In particular, the highest peak almost at the radius mid-point is due to the innermost (bowl-shaped) mirror. The receiver should then optimally begin at the mid-point between the center of the spheres and the mirrors and end close to the mirrors. However, due to the relatively low radiation that reaches the part of the receiver near the mirrors, it has been found that a reduction of the length of the receiver by an extra 40% in its lower part (closest to the mirrors) is beneficial. In fact, the radiation that is not collected is compensated by the reduction of thermal losses due to the lower receiver outer surface, and a lower capital cost due to the fact that the receiver will be smaller, which implies less material costs and working hours. In practice, given the radius of the prototype concentrator (15 m), the receiver could be in theory 7.5 m long (half radius), but due to the shortening of the lower part, the length can be further reduced to 4.5 m.

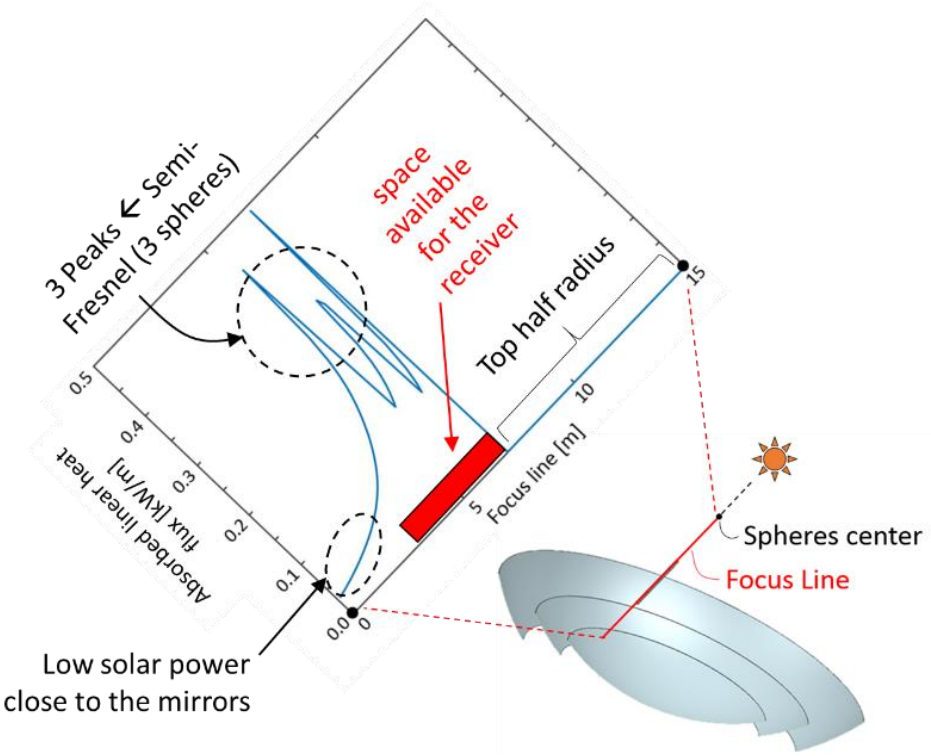

Figure 8. Axial distribution of the azimuthally integrated power [kW/m] from the mirrors (= 0 m) to the center of the spheres (= 15 m). The red rectangle qualitatively indicates the location and length of the receiver resulting from this optimization

The helix diameter is determined considering the spillage. Figure 9a shows that, obviously, the amount of concentrated radiation able to reach the receiver increases by increasing the helix diameter. Because of the relatively short path of the concentrated rays, a diameter of 0.25 m is enough to ensure negligible spillage (≈ 1% of the incoming radiation); however, due to the above-mentioned bending constraints, D will be chosen = 0.3 m.

In order to reduce the receiver surface (prone to heat losses), at fixed incident power, the spatial distribution of the radiation reflected by the semi-Fresnel spherical concentrator can be exploited by modifying the upper part of the receiver to create a conic-shaped upper part (opening angle θ, see Figure 6), as already done in the Auroville receiver (Van den Akker, 2004). In fact, the angle between the rays and the receiver axis is small in the upper part (the rays tend to become almost parallel to the axis); therefore, progressively increasing the helix diameter, resulting into a cone shape, allows intercepting the rays well in advance with respect to the cylinder (See Figure 9b).

The receiver design is performed considering the heat flux corresponding to the maximum incident solar power (April 11 at noon), hence looking for the limit thermal conditions in order to operate the prototype safely. The performance of the receiver when the heat flux is concentrated in parts of the receiver lower than the cone is not being affected by the existence of the conic upper part; they are only affected by the tube length that the HTF has to still go through, so the final design of the cone-shaped ending of the receiver has little to no effect when different flux distributions appear in the receiver surface.

Optical simulations (not shown here) confirm that the impact of θ on the solar power absorbed by the receiver is negligible; however, the larger θ is, the larger the receiver length reduction, since the radius at the cone base (upper part) is kept constant to 0.245 m not to have an excessive shadow on the solar field. Therefore, the main benefit in introducing the conical-shape on the top is to reduce the receiver length, i.e., the surface area to which radiative and convective heat losses are associated, the amount of material needed to build the receiver (which affects the capital cost) and the receiver weight (relaxing the constraints for the tracking system). The cone angle θ also plays a key role in determining the slope of the helical tubes, which decreases as the diameter of the helix progressively increases going up the cone. Therefore, increasing the cone angle leads to a decrease of the minimum slope, until one hits the above-mentioned 2° constraint. The minimum slope is also affected by N as shown in Figure 10a, from which one gets the maximum allowed value of θ for different values of N. Note that Figure 10a displays also the case in which

$N = 1$, although it violates one of the constraints listed above, to make it evident that using a single thread also violets the condition about the minimum slope.

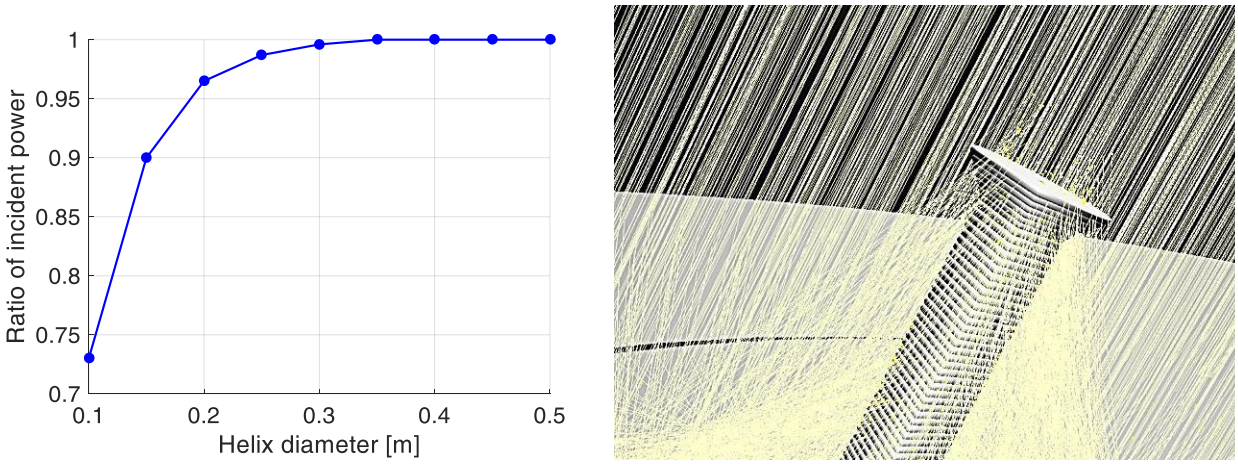

(a) (b)

Figure 9. (a) Fraction of the concentrated radiation that reaches the receiver for different helix diameters D. (b) Function of the conic part: rays that were incident on upper positions of a cylindrical receiver are now incident on the conic part. Note that, due to the graphical representation tools currently available in Tonatiuh, the receiver section seems squared, whereas the actual (circular) receiver shape is implemented in the optical model.

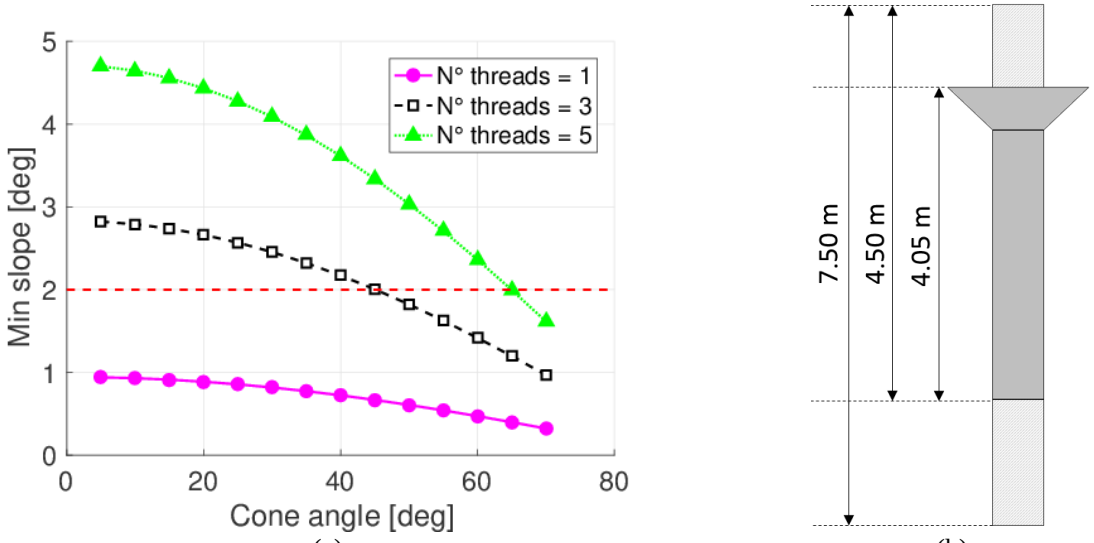

(a) (b)

Figure 10. (a) Minimum tube slope as a function of the number of threads and of the cone angle. The minimum acceptable value for the slope (2°) is highlighted with a red dashed line. (b) Receiver length: From half a radius (7.5 m) to 4.5 m removing the bottom part in view of the low heat flux and finally to about 4.05 m by including the conical insert on the top.

The final receiver length is therefore determined once the final value of the cone angle is defined. The latter depends as seen on the value of N that will be defined also on the base of the thermal-fluid-dynamic analysis (see section 3.3); thus, the final receiver length will be obtained only at the end of the design process (see section 3.4). Figure 10b shows the steps of the receiver shortening in the design process: starting from half of the bowl radius (7.5 m), which corresponds to the irradiated portion of the focus line, the length of the receiver is first reduced by 40% in its bottom

part, thanks to the low value of the concentrated heat flux there, while the top of the receiver is shortened by introducing a conical shape.

3.3 Thermal-fluid-dynamic analysis

The thermal-fluid-dynamic design aims at minimizing the heat losses by optimizing the diameter of the absorber tubes and the number of parallel threads. For this purpose, a quasi-3D thermal-fluid-dynamic dynamic model was developed in the Modelica language, following the approach presented in (Cagnoli et al., 2019). This model solves the 1D mass, momentum and energy balance of the internal flow of coolant (molten salts or thermal oil) and the axial and radial heat conduction in the absorber tube, while accounting for the convective heat transfer between the absorber tube and the coolant, as well as for the convective and radiative heat losses towards the environment.
The model allows simulating several absorber tubes in parallel, assuming that the coolant mass flow rate is evenly distributed among the tubes. Each helical tube is discretized by control volumes distributed along the axial direction (both internal flow and tube wall); a coarse azimuthal discretization is also considered that simply divides the tube wall in the front (irradiated) and back side (see Figure 11). Along the radial direction, the tube wall is discretized using three nodes (outer surface, midpoint and inner surface); the mass of the tube wall is lumped in the midpoint (see again Figure 11).
The thermal driver consists of the heat flux distribution on the absorber surface, as computed using the optical model. Particularly, the 3D heat flux (W/m2) distribution obtained by the optical model is processed in order to obtain, for each tube of the helical receiver, a 1D profile (along the tube axis) of the incident solar power (W/m). The other required boundary conditions for the coolant are the inlet temperature and mass flow rate and the pressure at the outlet; as far as the tube is concerned, the wind speed and the ambient temperature are required. On the outer surface, the radiative and convective (natural plus forced/wind) heat losses are computed on the base of suitable correlations. The back side of the tube is not irradiated and it is not directly exposed to the wind; thus, only losses by natural convection occur there; see Figure 11.

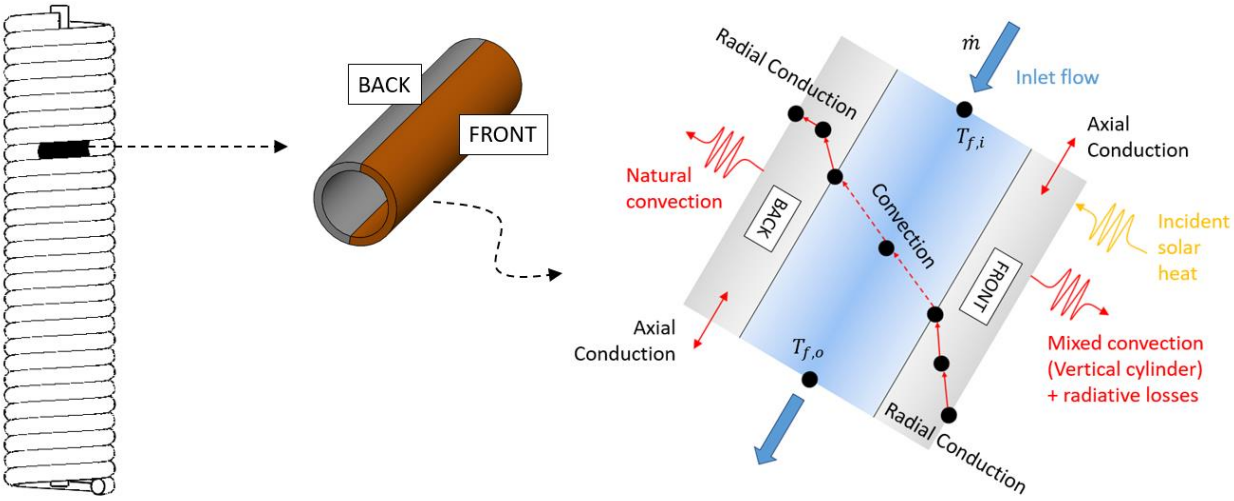

Figure 11. Scheme of a discretized control volume, highlighting the main heat transfer phenomena considered

3.3.1 Internal flow model

The mass, momentum and energy balance equations are solved for the internal flow. The dynamic continuity equation is computed as

$$\sum_j \left(A\Delta x \frac{d\rho}{dt} \right)_j = \dot{m}_{in} - \dot{m}_{out} \tag{2}$$

where, A is the tube cross section, Δx is the axial length of the *j-th* control volume (CV), ρ is the fluid density, $\dot{m}_{in}$ and $\dot{m}_{out}$ are the mass flow rate at the inlet and at the outlet of receiver, respectively, divided by the number of parallel absorber tubes. The continuity equation is solved only for the first tube since the mass flow rate is assumed to be evenly distributed among the tubes and the heat flux distribution is almost the same for each of the tubes.
The simplified (steady) momentum balance equation considered here is

$$\Delta p = \frac{1}{2}\left(f\frac{\Delta x}{d_i}\rho u^2\right)_j \tag{3}$$

where, Δp is the pressure drop across the control volume, d_i is the inner diameter of the tube and u is the speed of the fluid. The term f represents the friction factor, which has been determined by means of correlations suitable for curved tubes. Specifically, the Hart's correlation is adopted in the case of laminar flow and the White correlation in the case of turbulent flow (Hart et al., 1988). The flow regime has been determined comparing the average Reynolds number in the tube with a threshold value provided by the Srinivasan's correlation (Hart et al., 1988), which depends on both the diameter of the helix and that of the tube.
As for the mass balance, also the momentum balance is computed only for one tube due to the assumption of mass flow rate evenly distributed among the tubes.
The dynamic energy balance computed in the *j-th* control volume is

$$\left[A\Delta x\left(\rho c_p\frac{dT_{f,o}}{dt}+h_o\frac{d\rho}{dt}\right)\right]_j+\dot{m}_{in}(h_o-h_i)_j=Q_{f,j} \tag{4}$$

where c_p is the specific heat, $T_{f,o}$ is the fluid temperature at the CV outlet, ho and hi are the specific enthalpy at the inlet and outlet of the CV, respectively. Q_f is the heat transferred to the working fluid by convection with the inner tube wall (front and back side) computed with the Newton's cooling law. The needed heat transfer coefficient is computed by means of correlations suitable for curved tubes, according to the flow regime evaluated on the base of Srinivasan's correlation (Hart et al., 1988). Particularly, if the flow is turbulent the Roger and Mayew correlation is adopted, while the Schimdt correlation is used in the case of laminar flow (Sobota, 2011; Vashisth et al., 2008). Note that in Eq. 4 the specific kinetic and potential energy have been not considered since they are expected to be negligible if compared with the enthalpy increase. In the same way, the time derivative of the pressure is not included since it is expected to be negligible if compared with the time variations of temperature and density.

3.3.2 Energy balance in the solid

The tube wall model (front and back side) approximates the energy balance equation as

$$\frac{1}{2}A_s\Delta x_j\rho_w\left(c_w\frac{dT_w}{dt}\right)_j=Q_{axial,j}+Q_{radial,j} \tag{5}$$

where ρ_w is the wall density, c_w is the specific heat of the wall, dT_w is the wall temperature at the midpoint, A_s is the area of the tube wall cross section (annular region). The factor ½ is due to the fact that the tube wall is divided in the front and back side; therefore, only half of the tube cross section must be considered. The axial (Q_{axial}) and radial (Q_{radial}) conduction are computed both in the front (irradiated) and back wall. The heat conduction along the azimuthal direction is expected to be negligible (Rodríguez-Sánchez et al., 2014); thus, it is not considered in the model to save computational time. Given the thermal conductivity of the wall (k), the axial thermal conduction is approximated using the central difference scheme as

$$Q_{axial,j}=k_jA_s\frac{T_{w,j-1}-2T_{w,j}+T_{w,j+1}}{\Delta x_j} \tag{6}$$

To solve Eq. 6, it is assumed that the ends of the tube wall are adiabatic.
The radial thermal conduction takes into account the heat transferred between the midpoint and the outer surface and that transferred between the midpoint and the inner surface (see Figure 11); thus, it is written as

$$Q_{radial,j} = \left(\frac{1}{2}\right) 2\pi \Delta x_j k_j \left(\frac{T_{wo,j} - T_{w,j}}{log(d_o/d_{mid})} + \frac{T_{wi,j} - T_{w,j}}{log(d_{mid}/d_i)}\right) \quad (7)$$

where T_{wo} and T_{wi} are the wall temperatures on the outer and inner surface respectively, while d_o, d_{mid} and d_i are the tube diameters corresponding to the outer surface, midpoint and inner surface, respectively. The term ½ is again introduced to take into account that only half tube is considered, since it is divided in the front and back side.
On the inner surface, the heat transferred by radial conduction is imposed to be equal to that transferred by convection with the coolant (Q_f). On the outer surface of the tube, the heat transferred by radial conduction is equal to the solar absorbed power, net of the convective and radiative heat losses (front wall) or the heat lost by natural convection (back wall); see Eq. 8 and Eq. 9, respectively.

$$\left(\frac{1}{2}\right) 2\pi \Delta x_j k_j \left(\frac{T_{wo,j} - T_{w,j}}{log(d_o/d_{mid})}\right) = Q_{sun,j} - Q_{rad,j} - Q_{conv,j} \quad (8)$$

$$\left(\frac{1}{2}\right) 2\pi \Delta x_j k_j \left(\frac{T_{wo,j} - T_{w,j}}{log(d_o/d_{mid})}\right) = -Q_{conv,j} \quad (9)$$

The solar absorbed power is the imposed thermal driver, computed on the base of the optical model results. The radiative heat losses (Q_{rad}) from the front wall are calculated according to the Stefan-Boltzmann law. The temperature of the cold sink is assumed equal to the sky temperature, which is imposed to be 8 °C below the ambient temperature (Forristall, 2003). The model allows taking into account the presence of a surface coating by setting the desired surface emissivity as a function of the temperature. The convective heat losses (Q_{conv}) are evaluated on the base of the Newton's cooling law, which requires introducing a heat transfer coefficient. On the front wall, both the buoyancy effect (natural convection) and the presence of the wind (forced convection) has to be considered leading to the so-called mixed convection, while only losses by natural convection can occur on the back side. According to the work of Siebers (Siebers and Kraabel, 1984), which focuses on the convective heat losses from cylindrical external-type solar receivers for solar tower system, the heat transfer coefficient for mixed convection can be calculated as

$$HTC = \left(HTC_n^{3.2} + HTC_f^{3.2}\right)^{1/3.2} \quad (10)$$

where HTC_n is the heat transfer coefficient for natural convection estimated on the base of the correlation proposed by Siebers that applies to vertical flat plates, while HTC_f is the heat transfer coefficient for forced convection calculated on the base of the Churchill-Bernstein correlation for smooth cylinders in cross flow (Siebers and Kraabel, 1984). In the case of the back wall (only natural convection), the HTC_f is imposed to be zero. According to these correlations, the characteristic length is the helix diameter for the forced convection and the receiver length for the natural convection, assuming a vertical orientation of the receiver. A more accurate estimation of the mixed convective heat losses could be only obtained with a (computationally heavier) 3D CFD model able to consider the actual orientation of the receiver in the space and the presence of the solar field that affects the external (air) flow field.

3.4 Final design of the receiver prototype

The thermal-fluid-dynamic model has been applied to establish how the absorber tube diameter and the number of parallel threads affect the thermal performance of the receiver. For this purpose, a simplified circuit has been developed in Modelica (Figure 12), which imposes the required boundary conditions on the receiver, including mass flow rate source/sink and the computed heat flux distribution on the receiver surface, which acts as a driver.
The model is set up as follows:

- Receiver: the wall thickness is 1.5 mm, the tube material is Incoloy 800. The cone angle has been fixed to 40°; since it was checked that this parameter does not significantly affect the thermal performance. This is because the absorbed power is always the same and the receiver outer surface (prone to heat losses) changes negligibly with the cone angle, since it represents only a small part of the entire receiver. A surface coating (Pyromark 2500 (Ho et al., 2013)) is considered to increase the surface absorptivity.
- The ambient temperature is set to 20 °C and the condition of no wind (only natural convection) is considered with the receiver vertically oriented.

- The heat transfer fluid is a thermal oil (Helisol 5A), which replaces in the prototype the molten salts proposed for the MOSAIC system. Since the prototype aims at proving the MOSAIC concept, the imposed inlet temperature is 290 °C, which is the design inlet temperature for the MOSAIC module using molten salts. The mass flow rate is then controlled in order to obtain an outlet oil temperature equal to 450 °C (maximum oil temperature due to the degradation at high temperatures). Note that this temperature can only be achieved for short periods, while the nominal temperature for continuous operation is 425°C. In this case, the design conditions of the MOSAIC module (outlet temperature = 565 °C) cannot of course be reproduced.
- The thermal driver consists of the heat flux distribution computed by means of the optical model at the prototype site (Sangüesa, Spain); the day/hour (April 11 at noon) that leads to the maximum total incident power on the receiver was chosen. In this way, the receiver prototype will be designed considering the most severe thermal conditions, ensuring a safe operation of the prototype during the whole test campaign.

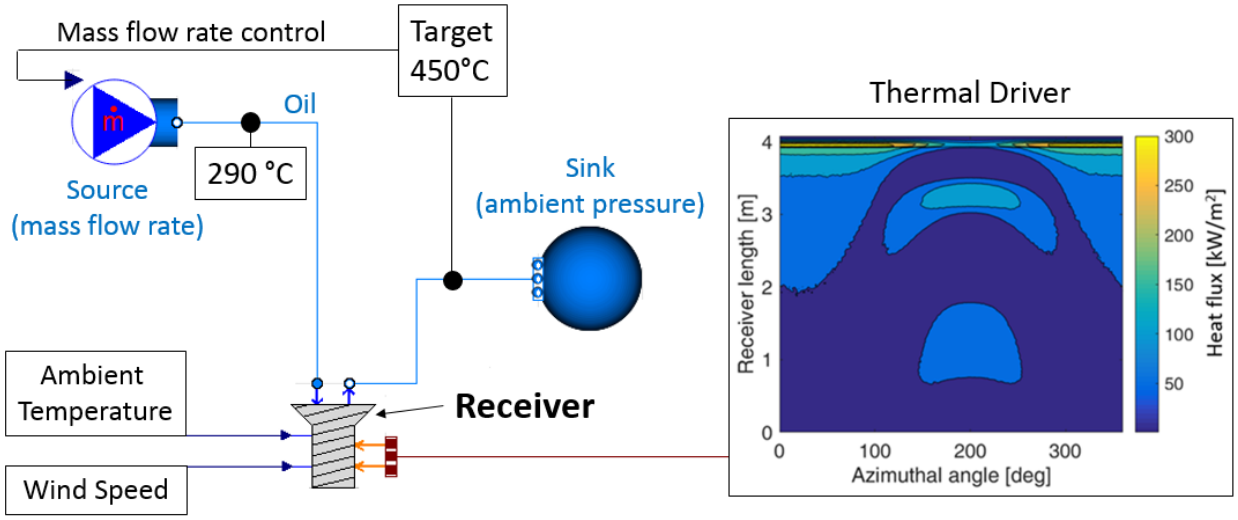

Figure 12. Imposing the boundary conditions for the steady-state prototype receiver analysis using Modelica

A parametric study was performed varying the "microscopic" parameters; namely the absorber pipe diameter d and the number of parallel threads *N*. The results have been evaluated in terms of receiver thermal efficiency, defined as

$$\eta = Q_f / Q_{abs} \tag{11}$$

where Q_{abs} is the absorbed solar power.
Figure 13 shows that the lower are the tube diameter and the number of parallel threads, the higher is the efficiency. Indeed, increasing *d* or *N* leads to a reduction of the oil Reynolds number and consequently of the heat transfer coefficient between the tube inner wall and the coolant. This negative effect is partially compensated by the reduction of the pressure drop, which decreases increasing the tube diameter and the number of threads (not shown). However, the power spent to circulate the oil in the receiver is orders of magnitude lower than the power associated with the enthalpy increase; for this reason, it is neglected in Eq. 11.

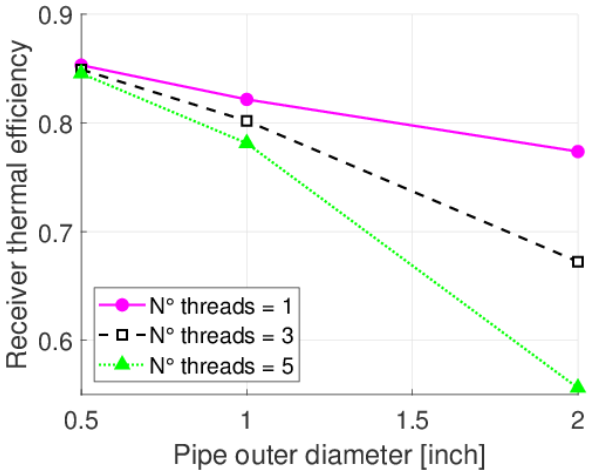

Figure 13. Receiver (prototype) thermal efficiency as a function of the helical tubes diameter and of the number of parallel threads

In conclusion, the minimum tube diameter and number of threads of the helix have to be adopted, compatibly with the manufacturing limits, which results in a tube diameter of 1" (lowest diameter easily available in the market) and three parallel helical tubes. Regarding the cone angle, for a triple-threaded receiver the maximum value to ensure drainage by gravity is 45°, see Figure 10a; thus, a cone angle of 40° was selected to have some margin. Figure 14a shows a CAD view of the final receiver prototype, while Figure 14b shows the real receiver during manufacturing at the workshop.

Looking at Figure 13, it can be concluded that the constraints applied to the receiver prototype design ($N \geq 3$ and $d \geq 1$") limit the thermal performance of the receiver. Ad hoc manufacturing processes, able to overcome these constraints, could be implemented in a large scale plant, where the size of the plant justifies the initial investment cost required to develop customized components.

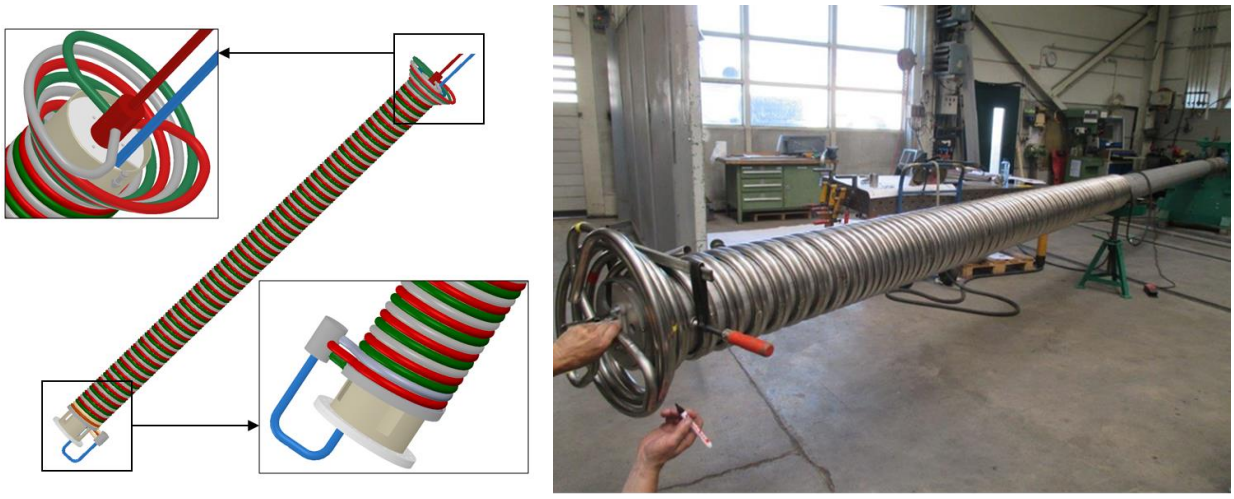

(a) (b)

Figure 14. (a) CAD view of the final receiver design, with the details of the conical part at the receiver top and of the bottom side of the receiver. The blue tube is feeding tube that pass inside the helix. (b) Receiver manufacturing at the AALBORG workshop.

4 Start-up (transient) analysis

Here, the aim is to evaluate the average rate of temperature increase, defined as the ratio between the steady-state to initial temperature difference and the time to steady state, which is a key parameter to assess the receiver thermo-

mechanical strength under fast changes of the heat flux (Zavoico, 2001). To simulate this start-up transient, the heat flux is linearly ramped-up from zero to the condition computed by the steady state optical analysis (Figure 15). Different ramp durations δ have been simulated ranging from 0 s (step function) to 240 s (above which the time to steady state coincides with δ). Severe ambient conditions (absence of wind), from the point of view of the wall temperature, were imposed. The ambient temperature was imposed equal to the maximum value expected in the prototype site (38 °C). A variation of the ambient temperature was checked not to lead to significant variations of the wall temperature. The inlet oil temperature is 290 °C and the mass flow rate is fixed at 0.69 kg/s, which is the maximum value that can be circulated in the thermal loop by the pumps.

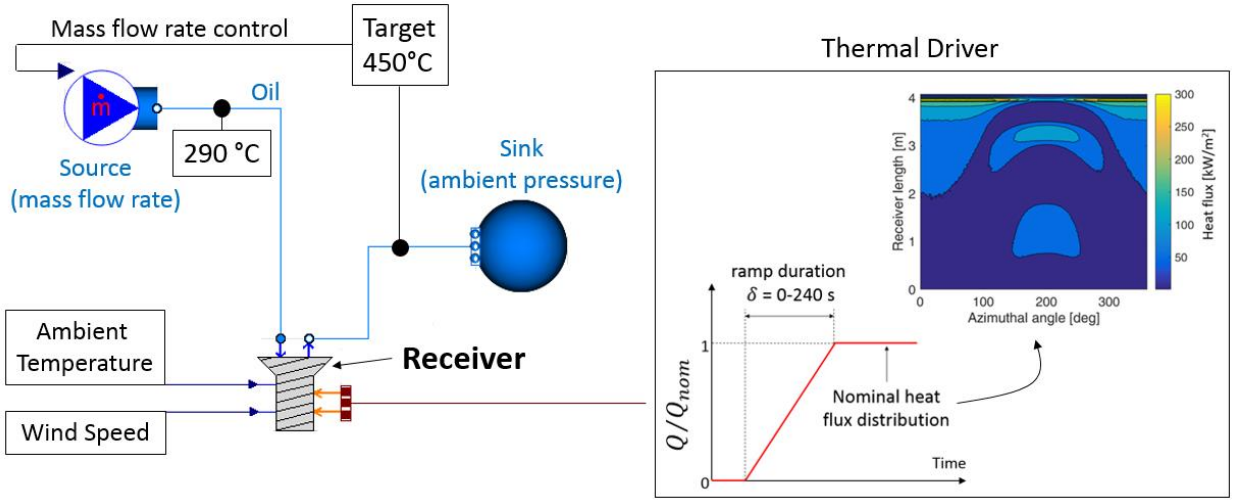

Figure 15. Modelica simulation environment for the analysis of the start-up (transient) scenario

Figure 16a shows the computed maximum wall temperature evolution during the transient for the two borderline cases of δ = 0 s and δ = 240 s. Figure 16b displays the rate of temperature increase as a function of the ramp duration. According to (Zavoico, 2001), the rate of temperature increase should be lower than 2.8 °C/s (about 168 °C/min). Therefore, the receiver operation strategy has to be planned considering that the heat flux on the receiver has to be progressively increased up to the nominal value and this process cannot be faster than about 90 seconds. This result has been confirmed by a dedicated simulation where the ramp-up approximation was replaced by the actual heat flux evolution along the receiver path from the parking position to the focus, which was imposed to last about 90 seconds. The computed temperature increases matched very well with the prediction obtained by the ramp approximation, being the result close to 168 °C/min.

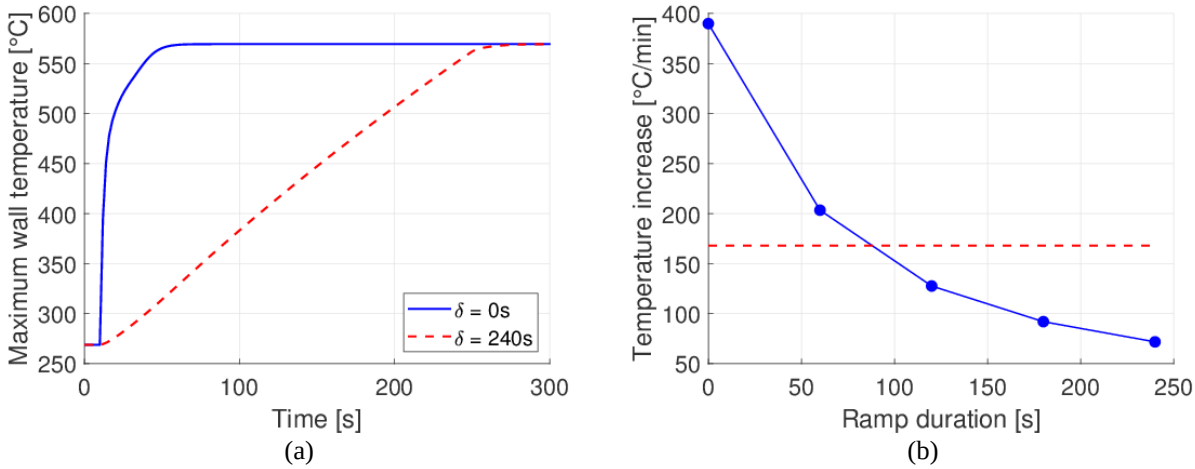

(a) (b)

Figure 16. (a) Maximum wall temperature evolution during the transient for δ = 0 s and δ = 240 s. (b) Rate of temperature increase as a function of the ramp duration. The threshold value (168 °C/min) is highlighted with a horizontal dashed line.

5 Conclusions and perspective

This paper presents the methodology developed for the design of the receiver of the innovative MOSAIC solar bowl prototype, now in the commissioning phase, which adopts a (stationary) semi-Fresnel spherical concentrator and a cable-based tracking system for the receiver.

The design methodology consists of three steps; first, in the preliminary design phase, the helical receiver configuration has been chosen among three alternatives. The receiver is provided with a conical insert on the top part (as already done in the Auroville solar bowl system) to better catch the solar radiation and consequently reduce the receiver length. The second step of the design methodology corresponds to the "macroscopic" sizing of the helical receiver, which is based on an optical model, developed using a Monte Carlo ray-tracing software that provides the heat flux distribution on the receiver surface for a given sun position. The computed heat flux distribution is strongly non-uniform and presents three peaks as a result of the semi-Fresnel configuration of the solar field. The optical model determines the "macroscopic" design parameters (diameter D and length L of the helix and cone angle θ) that define the receiver external size, which is mainly influenced by the spillage. The third, and last step of the design methodology is based on a dynamic thermal-fluid-dynamic model, leading to the optimization of the "microscopic" design parameters of the receiver, namely the absorber tubes diameter and the number of parallel threads, by means of steady-state simulations. These parameters directly affect the Reynolds number of the HTF flow and, consequently, the heat transfer coefficient between the internal flow and the tube wall, which is a key factor affecting the convective and radiative heat losses, i.e., the thermal performance of the receiver.

The above-mentioned, general design methodology has been applied in the paper to determine the best performing receiver prototype configuration for MOSAIC, while still respecting the manufacturing limits; the same methodology presented here can be applied to the full-scale receiver. The manufacturing limits and the constraints applied to the prototype design could likely be overcome in a large scale plant, which may justify the cost of developing ad-hoc manufacturing processes and a customization of the components (e.g. the diameter of the absorber tubes), in view of the large quantities ordered. In addition, an analysis in transient conditions has been performed, which shows that the start-up of the system requires increasing the heat flux on the receiver up to the nominal value in not less than about 90 seconds, to avoid excessive thermal stresses during the test of the prototype.

Besides the demonstration of the innovative solar bowl technology, the forthcoming test of the MOSAIC prototype will allow the validation of the models presented here against the experimental data that will be collected.

Acknowledgments

This project has received funding from the European Union's Horizon 2020 research and innovation programme under the Grant Agreement Nº 727402.

References

Awasthi, K., Khan, M.K., 2019. Performance evaluation of coiled tube receiver cavity for a concentrating collector. Renew. Energy 138, 666–674. doi:10.1016/j.renene.2019.02.015

Blanco, M.J., Amieva, J.M., Mancilla, A., 2005. The Tonatiuh Software Development Project: An open source approach to the simulation of solar concentrating systems, in: Proceedings of the ASME Computers and Information in Engineering Division. pp. 157–164. doi:10.1115/IMECE2005-81859

Cagnoli, M., de la Calle, A., Pye, J., Savoldi, L., Zanino, R., 2019. A CFD-supported dynamic system-level model of a sodium-cooled billboardtype receiver for central tower CSP applications. Sol. Energy 177, 576–594.

Cohen, S., Grossman, G., 2016. Development of a solar collector with a stationary spherical reflector/tracking absorber for industrial process heat. Sol. Energy 128, 31–40. doi:10.1016/j.solener.2015.05.036

Fernández, A.G., Gomez-Vidal, J., Oró, E., Kruizenga, A., Solé, A., Cabeza, L.F., 2019. Mainstreaming commercial CSP systems: A technology review. Renew. Energy 140, 152–176. doi:10.1016/j.renene.2019.03.049

Forristall, R., 2003. Heat Transfer Analysis and Modeling of a Parabolic Trough Solar Receiver Implemented in Engineering Equation Solver. Technical Report, NREL/TP-550-34169, National Renewable Energy Laboratory.

Fruchter, E., Grossman, G., Kreith, F., 1982. An experimental investigation of a stationary reflector/tracking absorber solar collector at intermediate temperatures. J. Sol. Energy Eng. Trans. ASME 104, 340–344. doi:10.1115/1.3266327

Hart, J., Ellenberger, J., Hamersma, P.J., 1988. Single- and two-phase flow through helically coiled tubes. Chem. Eng. Sci. 43. doi:10.1016/0009-2509(88)80072-1

Ho, C.K., Mahoney, A.R., Ambrosini, A., Bencomo, M., Hall, A., Lambert, T.N., 2013. Characterization of Pyromark 2500 Paint for High-Temperature Solar Receivers. J. Sol. Energy Eng. 136, 014502. doi:10.1115/1.4024031

IEA International Energy Agency, 2018. World Energy Outlook.

IRENA International Renewable Energy Agency, 2018. Renewable Power Generation Costs in 2017. Abu dhabi.

Islam, M.T., Huda, N., Abdullah, A.B., Saidur, R., 2018. A comprehensive review of state-of-the-art concentrating solar power (CSP) technologies: Current status and research trends. Renew. Sustain. Energy Rev. 91, 987–1018. doi:10.1016/j.rser.2018.04.097

Maatallah, T., Houcine, A., El Alimi, S., Ben Nasrallah, S., 2018. A novel solar concentrating system based on a fixed cylindrical reflector and tracking receiver. Renew. Energy 117, 85–107. doi:10.1016/j.renene.2017.10.040

McIntosh, A.D., 1990. An equation for the caustic curve. Phys. Educ. 25. doi:10.1088/0031-9120/25/3/413

MOSAIC, 2019. MOSAIC H2020 Project [WWW Document]. URL https://mosaic-h2020.eu/ (accessed 11.17.19).

O'Hair, E.A., Green, B.L., 1992. Solar bowl component efficiencies. J. Sol. Energy Eng. Trans. ASME 114, 272–274. doi:10.1115/1.2930017

Pye, J., Coventry, J., Venn, F., Zapata, J., Abbasi, E., Asselineau, C.A., Burgess, G., Hughes, G., Logie, W., 2017. Experimental testing of a high-flux cavity receiver, in: AIP Conference Proceedings. pp. 110011 1–8. doi:10.1063/1.4984485

Rodríguez-Sánchez, M.R., Soria-Verdugo, A., Almendros-Ibáñez, J.A., Acosta-Iborra, A., Santana, D., 2014. Thermal design guidelines of solar power towers. Appl. Therm. Eng. 63, 428–438. doi:10.1016/j.applthermaleng.2013.11.014

Siebers, D.L., Kraabel, J.S., 1984. Estimating Convective Energy Losses From Solar Central Receivers - Report N. SAND84-8717. Albuquerque, New Mexico, USA.

Sobota, T., 2011. Experimental Prediction of Heat Transfer Correlations in Heat Exchangers, in: Dos Santos Bernardes, M.A. (Ed.), Developments in Heat Transfer. Intechopen.

Solar Cookers International, 2019. Auroville Solar Kitchen [WWW Document]. URL https://solarcooking.fandom.com/wiki/Auroville_Solar_Kitchen (accessed 11.17.19).

Stine, W., Geyer, M., 2001. Concentrating Collectors, in: Power from the Sun.

Texas Tech University, 2019. Texas Tech University Crosbyton Solar Power Project 65 Foot Diameter Solar Gridiron. [WWW Document]. URL https://swco-ir.tdl.org/handle/10605/417 (accessed 11.17.19).

Van den Akker, J., 2004. The Power of Human Unity - Renewable Energy in Auroville. Renew. Energy Focus 26–29.

Vashisth, S., Kumar, V., Nigam, K.D.P., 2008. A review on the potential applications of curved geometries in process industry. Ind. Eng. Chem. Res. 47, 3291–3337. doi:10.1021/ie701760h

Villasante, C., Herrero, S., Sánchez, M., Pagola, I., Peña, A., Olasolo, D., Bernardos, A., 2020. Low-Cost Solar Electricity Using Stationary Solar Fields; Technology Potential and Practical Implementation Challenges to Be Overcome. Outcomes from H2020 MOSAIC Project. Energies 13. doi:10.3390/en13071816

Villasante, C., Pagola, I., Peña, A., Sánchez, M., Olarra, A., Gomez-Acedo, E., Herrero, S., 2019. "MOSAIC", A new CSP plant concept for the highest concentration ratios at the lowest cost, in: AIP Conference Proceedings. doi:10.1063/1.5117594

Zavoico, A., 2001. Solar Power Tower: Design Basis Document - Report SAND2001-2100. San Francisco, California, USA.